Hand function after neonatal stroke: a graph model based on basal ganglia and thalami structure

Patty Coupeau, Josselin Démas, Jean-Baptiste Fasquel, Lucie Hertz-Pannier, Stéphane Chabrier, Mickael Dinomais

Hand function after neonatal stroke: a graph model based on basal ganglia and thalami structure

Patty Coupeau,[1] Josselin Démas,[1,2] Jean-Baptiste Fasquel,[1] Lucie Hertz-Pannier, [3] Stéphane Chabrier, [4] and Mickael Dinomais[1,5]

Author affiliations:

1 Université d'Angers, LARIS, SFR MATHSTIC, F-49000 Angers, France

2 Instituts de Formation, CH Laval, France

3 UNIACT/Neurospin/JOLIOT/DRF/CEA-Saclay, and U1141 NeuroDiderot/Inserm, CEA, Paris University, France

4 French Centre for Pediatric Stroke, Pediatric Physical and Rehabilitation Medicine Department, Saint-Etienne University Hospital, France

5 Department of Physical and Rehabilitation Medicine, University Hospital, CHU Angers, France

Correspondence to: Patty Coupeau

LARIS – Polytech Angers, 62 avenue de Notre Dame du Lac 49000 ANGERS
patty.coupeau@univ-angers.fr

Running title: Graph-based motor prediction after NAIS

Abstract

Introduction: Neonatal arterial ischemic stroke (NAIS) is a common model to study the impact of a unilateral early brain insult on developmental brain plasticity and the appearance of long-term outcomes. Motor difficulties that may arise are typically related to poor function of the affected (contra-lesioned) hand, but surprisingly also of the ipsilesional hand. Although many

longitudinal studies after NAIS have shown that predicting the occurrence of gross motor difficulties is easier, accurately predicting hand motor function (for both hands) from morphometric MRI remains complicated. The hypothesis of an association between the structural organization of the basal ganglia (BG) and thalamus with hand motor function seems intuitive given their key role in sensorimotor function. Neuroimaging studies have frequently investigated these structures to evaluate the correlation between their volumes and motor function following early brain injury. However, the results have been controversial. We hypothesize the involvement of other structural parameters.

Method: The study involves 35 children (mean age 7.3 years, SD 0.4) with middle cerebral artery NAIS who underwent a structural T1-weighted 3D MRI and clinical examination to assess manual dexterity using the Box and Blocks Test (BBT). Graphs are used to represent high-level structural information of the BG and thalami (volumes, elongations, distances) measured from the MRI. A graph neural network (GNN) is proposed to predict children's hand motor function through a graph regression. To reduce the impact of external factors on motor function (such as behavior and cognition), we calculate a BBT score ratio for each child and hand.

Results: The results indicate a significant correlation between the score ratios predicted by our method and the actual score ratios of both hands ($p < 0.05$), together with a relatively high accuracy of prediction (mean L1 distance < 0.03). The structural information seems to have a different influence on each hand's motor function. The affected hand's motor function is more correlated with the volume, while the 'unaffected' hand function is more correlated with the elongation of the structures. Experiments emphasize the importance of considering the whole macrostructural organization of the basal ganglia and thalami networks, rather than the volume alone, to predict hand motor function.

Conclusion: There is a significant correlation between the structural characteristics of the basal ganglia/thalami and motor function in both hands. These results support the use of MRI macrostructural features of the basal ganglia and thalamus as an early biomarker for predicting motor function in both hands after early brain injury.

Keywords: perinatal stroke; cerebral palsy; motor cortex; basal ganglia; structural organization; graph neural network

1. Introduction

With a birth prevalence of 37-67/100,000 (mostly term-born), perinatal stroke appears as a general term encompassing "*heterogeneous conditions with a focal cerebral arterial or venous occlusion, occurring between 20 weeks of fetal life through 28th postnatal day*" (Raju, Nelson, Ferriero, & Lynch, 2007). Among the six main perinatal stroke syndromes, which differ according to various factors (causality, mechanism, time of onset, and mode of presentation of the brain insult), Neonatal Arterial Ischemic Stroke (NAIS) is the most prevalent type, with an estimated incidence of 1 in 3000 term births. NAIS is defined as a symptomatic cerebral arterial ischemic insult occurring within the first 4 weeks of life (Fluss, Dinomais, & Chabrier, 2019).

NAIS is one of the most extensively studied perinatal strokes and serves as a paradigm for other entities. The lesion and its timing are well defined in cases of NAIS, making it a unique model for studying the impact of a unilateral early brain insult on developmental brain plasticity (Kirton, 2013) related to the appearance of long-term outcomes. The rate of unilateral cerebral palsy (CP) (Chabrier, et al., 2019) among term infants with NAIS is close to 30%. Hence, NAIS is a leading cause of unilateral CP predominantly affecting the left hemisphere (Craig, Carlson, & Kirton, 2019). The middle cerebral artery (MCA) is the most frequently affected vascular territory. Direct damage to the basal ganglia and/or thalamus typically does not occur in NAIS in the MCA territory, even if in cases of proximal M1 occlusion, damage to the basal ganglia can occur. Additionally, long-term direct or indirect structural alterations of these structures have been described in both hemispheres following NAIS (Craig, Carlson, & Kirton, 2019) (Hassett, Carlson, Babwani, & Kirton, 2022).

Though all children with unilateral CP after NAIS can walk, their motor difficulties are mostly related to the poor function of the affected (contra-lesioned) hand. Surprisingly, the ipsilesional hand (theoretically referred to as the 'unaffected' hand) also often exhibits abnormal function in these children (Kuczynski, Kirton, Semrau, & Dukelow, 2018). The neuroscientific rational (neural substratum) for this phenomenon is not yet clear.

If neonatal and long-term brain imaging can be used to predict the presence or absence of CP (and a broad range of motor outcomes) (Dinomais, et al., 2015) (Dinomais, et al., 2016), determining the severity of hand functional impairment is much more challenging. The occurrence of CP is related to lesion characteristics (location and extent of the infarct), as well as the involvement of the cortico-spinal tract at any level, much more than the size of the infarct (Dinomais, et al., 2015) (Dinomais, et al., 2016). Follow-up studies after NAIS have shown

that predicting the occurrence of CP and gross motor difficulties is relatively straightforward. Accurately predicting hand motor function in both the affected and 'unaffected' hands from morphometric MRI remains a complex task. Indeed, many studies have provided conflicting or sparse results (Dinomais, et al., 2016) (Craig, Carlson, & Kirton, 2019) (Hassett, Carlson, Babwani, & Kirton, 2022) (Ilves, et al., 2022).

Analyzing the hypothesis for an association between the volumes of the basal ganglia (BG) and thalamus with hand motor functions seems intuitive considering the key role of the basal ganglia and thalamus in sensorimotor function (Arsalidou, Duerden, & Taylor, 2013). In addition, the important postnatal growth (Gilmore, et al., 2012) (Raznahan, et al., 2014) (Makropoulos, et al., 2016) and developmental susceptibility of these deep gray matter structures to brain insults make them perfect candidates for explaining hand motor function after NAIS.

Until recently, these structures have often been explored in detail per-se in neuroimaging studies to assess their relationship with motor function following early brain injury, with controversial results. Ilves et al. (Ilves, et al., 2022) demonstrated that children after ischemic perinatal stroke have a smaller ipsilesional thalamus and putamen, which correlates with affected hand function. Craig et al. (Craig, Carlson, & Kirton, 2019) did not find this association for the thalamus. Interestingly, Hasset et al. (Hassett, Carlson, Babwani, & Kirton, 2022) also found an association between the volume of the ipsilesional putamen and affected hand function, without analyzing the volume of the thalamus, yet closely linked to basal ganglia in brain motor function.

Even more controversial results exist regarding the link between basal ganglia volume changes and 'unaffected' hand function (Craig, Carlson, & Kirton, 2019) (Ilves, et al., 2022). Currently, there is no distinct correlation between clinical motor outcomes and thalamic and/or basal ganglia volumes, in either affected or 'unaffected' hands (ipsi- or contra-lesioned hemisphere).

These studies focus solely on the relationship between the volume of these brain structures and motor functions. It is widely accepted that there is a positive correlation between brain structure volume and function (e.g., with intelligence (Pietschnig, Penke, Wicherts, Zeiler, & Voracek, 2015)). However, many neuroimaging studies have reported discordant relationships between brain volumes and brain functions, with both increased and/or decreased volumes of brain structures associated with better outcomes (Peterson, et al., 2000) (Hollander, et al., 2005). This suggests that interpretation of the relationship between regional brain volumes and brain

functions is difficult. Considering the complex anatomies of the basal ganglia and thalamus, as well as their complex inter-relationship with the cortex (cortico-basal ganglia-thalamo-cortical network), analyzing the association between motor function and only volumes of the BG and/or thalamus appears as an overly simplistic approach. This may the reason why studies did not find a consistent relationship between thalamic/BG volumes and long-term hand motor function following NAIS.

Thus, to figure out the relationship between long-term hand motor function and the characteristics of BG/thalami, we hypothesize the involvement of other structural parameters besides volume (see infra), which can characterize stroke-related atrophy.

A recent study showed that deformation of brain structure is a more sensitive measure of function than volume, and that basal ganglia distortion may be a neurophenotype for risk of developmental disorders (Sandman, et al., 2014). More specifically, they showed that the expansion and contraction of the putamen is more predictive of intellectual quotient than its volume itself. In this sense, we propose to assess the relationship between children's clinical motor outcome and the structural organization of the thalamus and basal ganglia, using other values that characterize the deformation of structures. We consider the elongation of the basal ganglia and thalamus to determine if an expansion or contraction of these structures affects children's hand motor function. We assume that the structural loss of brain structures after NAIS due to Wallerian degeneration, specifically the thalamus (as previously demonstrated (Dinomais, et al., 2016), will potentially be accompanied by a deformation (contraction) that can be characterized with the elongation parameter. To quantify deformation of the basal ganglia of different nature than contraction, we also considered the distance between the centroids of these structures. Indeed, the displacement of structure's centroid is expected when it is deformed due to volume loss of other brain structures. By calculating the distance between centroids, we aim to indirectly capture the effect of atrophy in hemispheres that modify the structural relationship between BG/thalami. Specifically, we can assume that the inter-hemispheric distance between centroids will be modified if the injured hemisphere has atrophied.

Graphs are commonly used to represent this kind of high-level structural information. Each node in the graph describes a region of the brain (volume and elongation of a brain structure in our case) and edges carry structural information between these regions (distances in our case). Graph representation makes it possible to highlight the inter-hemispheric structural

relationships and variations by connecting structures with edges. Recently, many graph neural network (GNN) architectures have been developed to perform different tasks like graph classification, graph regression, or node classification (Bacciu, Errica, Micheli, & Podda, 2020). Predicting hand motor function (assessed by Box and Block tests) can be considered a graph regression problem, attempting to predict hand motor function from a graph representing the structural organization of the basal ganglia and the thalamus. GNN-based strategies are becoming increasingly popular in the medical field. Thus, recently, GNNs were utilized for graph regression to predict IQ scores from graphs that represent brain connectivity (Hanik, Demirtaş, Gharsallaoui, & Rekik, 2022). In previous work, we introduced a GNN-based classification model for predicting cerebral palsy in children with NAIS (Coupeau, Fasquel, Démas, Hertz-Pannier, & Dinomais, 2023). Here, we aim to enhance by incorporating shape information (elongation of the structures) to predict hand motor function.

Based on the combined elements described above, including the important growth of BG and thalamus after birth, their key role in the motor system, as well as the impact of other morphological and structural parameters than volumes on clinical function, we hypothesize that children, at 7 years of age, after NAIS in the MCA territory, would have changes in the structural graph representation of the BG and thalamus related to the function of both hands (affected and 'unaffected' hands).

The objective of this study is to predict gross motor function evaluated by the Box and Blocks Test (Jongbloed-Pereboom, Nijhuis-van der Sanden, & Steenbergen, 2013) for both hands using a neural network that operates on graphs representing the macrostructural organization of the basal ganglia and thalamus. The aim is to assess the potential use of macrostructural characteristics, including elongation and distances (not limited to volume), of the basal ganglia and thalamus in MRI as an early biomarker for predicting motor function in both hands after early brain lesion.

2. Materials and methods

2.1. Participants

All patients participated in the French AVCnn cohort study (Clinical trial NCT02511249), which follows 100 term-born children with NAIS (Chabrier, et al., 2010) (Husson, et al., 2010). The diagnosis was based on the 2007 definition of NAIS: 1) acute neurological symptoms

within the first 28 days of life and 2) accompanied by correlated cerebral imaging findings, i.e., an ischemic lesion in an arterial territory (Raju, Nelson, Ferriero, & Lynch, 2007). All children were enrolled in 37 French hospitals from November 2003 to October 2006. A cross-sectional clinical and imaging analysis was conducted when the children reached the age of 7 (Dinomais, et al., 2015) (Dinomais, et al., 2016).

As part of the clinical follow-up, an experienced clinician, either a pediatric neurologist or a pediatric rehabilitation specialist, examined all children during the 7-year assessment. This examination included a developmental evaluation and a magnetic resonance imaging (MRI) investigation. 73 children were available for follow-up examinations and 52 for MRI. To ensure a homogeneous distribution of lesion characteristics, only the 37 children with a unilateral lesion in the middle cerebral artery territory, were selected as subjects for this study (Dinomais, et al., 2015). Two scans were excluded due to severe motion artifacts, which prevented the basal ganglia segmentation, leaving 35 participants as the study population.

For the computation of edge properties (related to distances) during graph construction (described later), we included in the study 31 control children aged 7 years who were available for an MRI scan. Control children were recruited on the basis that they should be between 7 and 8 years old, born at term, without chronic pathology, developmental disorders, or delays, and not taking any medication or experiencing neurological pathology. These same child controls have already been included in previous papers (Al Harrach, et al., 2019) (Al Harrach, et al., 2021).

Head circumference was measured using a tape measure and handedness of children was assessed according to the Edinburgh inventory (Oldfield, 1971). General characteristics of the participants are presented in Table 1.

2.2. Ethics

All patients and their parents gave written informed consent. Approvals from the local ethics committees were obtained by the Ethical Committee of the Saint-Étienne University Hospital (biomedical research 1008026) in June 2010.

Table 1. General profile of the participants

	Controls	**NAIS**	
		Left injured	**Right injured**
Number	n=31	n=20	n=15
	Mean (std) or n (%)	**Mean (std) or n (%)**	**Mean (std) or n (%)**
Age (years)	7.71 (±0.54)	7.32 (±0.45)	7.28 (±0.20)
Gender	Males: 16 (51,61%) Females: 15 (48,39%)	Males: 11 (55%) Females: 9 (45%)	Males: 10 (66.67%) Females: 5 (33,33%)
Right-handed	28 (90,32%)	5 (25%)	14 (93,33%)
Lesion size (mL)	-	59.06 (±82.05)	38.16 (±46.95)
Total Intracranial Volume	1,398.01 (±109.10)	1,278.16 (±173.57)	1,277.66 (±98.30)
Head circumference (cm)	52.50 (±1.16)	51.60 (±1.64)	51.10 (±1.43)
BBT score (affected / "unaffected" hand)	-	27.9 (±10.91) / 31.3 (±7.6)	28.2 (±6.66) / 31.9 (±5.40)

Abbreviations: BBT= Box and Blocks Test.

2.3. Data availability

The data that support the findings of this study are available from the corresponding author, upon reasonable request, according to the French legislation.

2.4. MR Image acquisition

All structural MRI T1-weighted 3D images were acquired with a 3.0 Tesla scanner (MAGNETOM TrioTim system, Siemens, Erlangen, Germany, 12 channel head coil) at Neurospin, CEA-Saclay, France (Dinomais, et al., 2015). Anatomical imaging using a T1-weighted magnetization-prepared rapid acquisition gradient-echo sequence [176 slices, repetition time (TR) 2300ms, echo time (TE) 4.18ms, field of view (FOV) 256, flip angle = 9°, voxel size 1mm×1mm×1mm] was acquired to obtain high-resolution T1 weighted image of the whole brain. Additionally, a 3D FLAIR sequence [160 slices, TR 5000ms, TE 395ms, FOV 230 mm, voxel size 0.9mm×0.9mm×1mm] was acquired on the same scanner. The co-registered 3D FLAIR images were used as a visual aid for the precise manual segmentation of the basal ganglia, as described in the next section.

2.5. Basal ganglia segmentation

Major nuclei within the basal ganglia complex include the putamen, the caudate nucleus (collectively termed the striatum), and the pallidum. To extract these structures along with the thalamus on the co-registered 3D T1 MRI, we combined a manual segmentation and an atlas-based segmentation using the Hammersmith atlas (Hammers, et al., 2003). Statistical Parametric Mapping version 12 (SPM12) software (Welcome Department of Imaging Neuroscience, University College, London, UK) was used to obtain the tissue probability map (TPM) of each control subject (T1 MRI) in the native space. We constructed a group template of the control 7-year-old children from their TPM using the DARTEL tool. We segmented the basal ganglia and the thalamus in the MNI space using the Hammersmith atlas. The T1-weighted volume of each subject (control and NAIS) was registered into the DARTEL template of 7-year-old children using the CAT12 tool. We thus obtained the deformation fields from each subject's native space into the Dartel template space, necessary to obtain the segmentation of basal ganglia and thalamus in the native space of each child. Then, the MRI segmentation was manually corrected slice by slice with *ITKSnap* (Yushkevich, Gao, & Gerig, 2016), using the co-registered FLAIR sequence to precisely segment the BG. Each segmentation was visually checked and validated through consensus with a specialist (MD).

2.6. Motor assessment

The Box & Blocks Test (BBT) (Jongbloed-Pereboom, Nijhuis-van der Sanden, & Steenbergen, 2013) was considered to evaluate manual dexterity. This test is commonly used in clinical trials and experimental research to measure hand dexterity. The BBT consists of a box with two compartments separated in the middle. At the beginning, 100 small blocks are in one of the compartments, on the same side of the tested hand. Children move as many cubes as they can from one compartment to the other. The hand function score is calculated based on the number of cubes moved into the second compartment within one minute. The higher the score, the better the hand function. Both the ipsi-lesional hand (i.e., the 'unaffected' hand) and the contra-lesional hand (i.e., the 'affected' hand) were evaluated. BBT scores for both hands are reported in Table 1. We calculated a BBT score ratio (described later) for each child and each hand to reduce the impact of other factors external to motor function (behavior, cognition, etc.) that can lead to variations in the BBT score. We hypothesize that these factors affect both hands equally. Thus, by calculating this ratio, we aim to reduce the impact of these confounding parameters

and test hand motricity more precisely. Note that the control participants did not undergo any hand motor function tests.

2.7. Graph construction

From the basal ganglia segmented in the MRI scans of children, we constructed the corresponding graphs. We defined a graph $G = (V, E, X, L)$ where V is the set of nodes (each node $v \in V$ corresponds to a basal ganglia or thalamic structure) and E is the set of edges. To study inter-hemispheric structural relationships between supposedly symmetrical structures, we coupled the structures pairwise (i.e., left caudate with right caudate, etc.). The inter and intra-hemispheric structures are not connected by an edge to avoid interfering with the GNN by providing misleading information (e.g., comparing the volume of the right thalamus to that of the right caudate). The topology of the constructed graphs is illustrated in Figure 1.

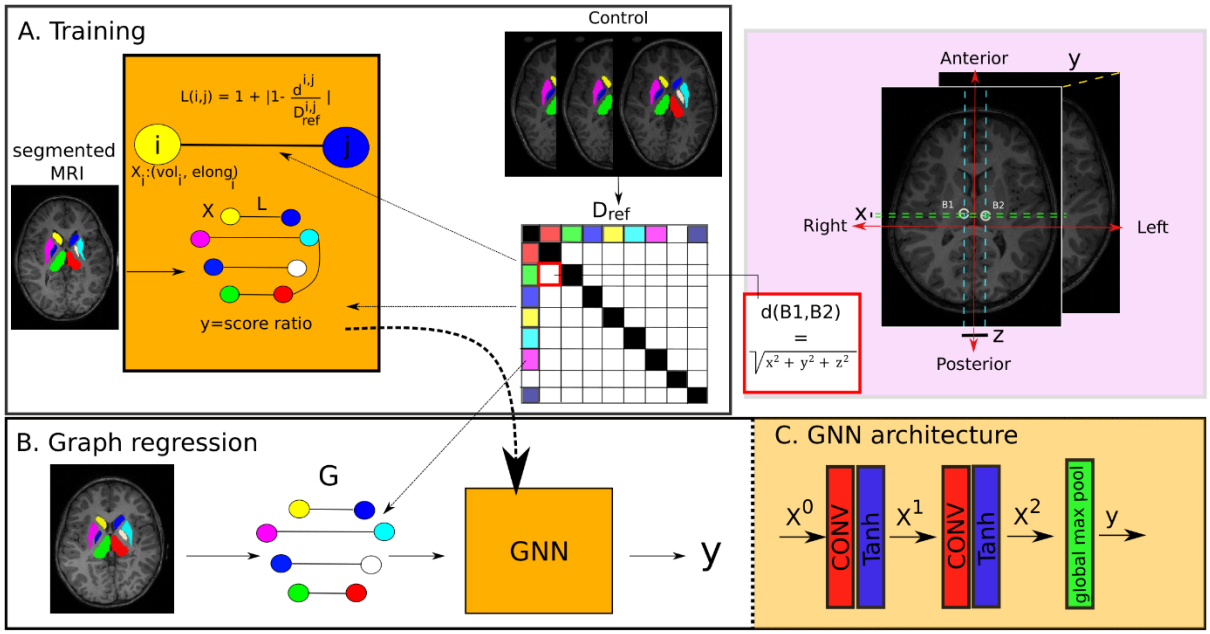

Figure 1. Illustration of the proposed method for predicting BBT score ratio (y) based on a regression graph neural network. (A): From the segmented MRI, a graph is constructed so that each node of the graph represents a brain structure. Nodes carry information related to the volume and elongation of the structure (vector X), while edges carry a ratio (scalar L) of the Euclidean distance (d) between the two connected structures in the studied child and of the mean Euclidean distance between these same two structures in a population of controls (stored in a matrix D_{ref}). (B): The graphs generated from the MRI of the training dataset are used to train the graph neural network (GNN) for predicting the BBT score ratio of new children based on their MRI. (C): The GNN architecture comprises of two convolution layers (CONV) followed by a hyperbolic tangent activation function (Tanh) and a global pooling layer based on the maximum value of the graph nodes at the output of the convolution.

X is a node attribute assignment function $X: V \rightarrow R^2$ regarding the volume (normalized to the total brain volume) and the elongation (normalized to the head circumference) of the corresponding structure. We extract each region of the segmented MRI using the Python (version 3.7) library *scikit-image*. We recovered the area of each structure and the major axis of the ellipse with the same normalized second central moments as the structure using the *regionprops* function of *scikit-image* library. The structure's volume was calculated by multiplying its area with the image resolution (1x1x1mm^3 for our dataset). Elongation was determined by measuring the length of the major axis of the extracted ellipse that encompasses the brain structure.

L is an edge attribute assignment function $L: E \rightarrow R$ relative to the distance between the centroids of the connected structures. More concretely, edges carry a distance-to-average ratio in healthy controls:

$$L(i,j) = 1 + |1 - \frac{d^{i,j}}{D_{ref}^{i,j}}| \qquad (1)$$

where $d^{i,j}$ indicates the Euclidean distance between the centroid of structures i and j in the 3D space and $D_{ref}^{i,j}$ represents the average Euclidean distance between the centroid of the structures i and j for control children. $D_{ref}^{i,j}$ is previously constructed, from the MRI of the 31 control children, as the average Euclidean distance between the centroids of each segmented structure. Thus, in Figure 1, the red box in D_{ref} indicates the control average Euclidean distance between the centroids B_1 and B_2 of the right and left thalamus in 3D space. To measure the distance between brain structures carried by $d^{i,j}$ and $D_{ref}^{i,j}$, we considered the Python library *scikit-image*. We recovered the 3D coordinates of the centroid of each segmented region (i.e. structure) of the MRI using the *regionprops* function of this library. We computed, using Python, the distance between the centroids of the connected regions along the 3 axes and multiplied it by the image resolution. From this distance along the 3 axes (in mm), we calculated the Euclidean distance. The edge attributes are computed to ensure they are greater than one (eq.1), avoiding too small values (close to zero) which would cancel out the node attributes during the convolution operation of the graph neural network (detailed below).

Each graph is associated with a Box and Blocks Test score ratio y, to be predicted. For each child, we studied the prediction of the score for the affected hand *LH* and the score for the

'unaffected' hand CLH obtained in the BBT. Therefore, two score ratios are considered for the prediction task:

$$y_1 = \frac{LH}{LH+CLH} \qquad (2)$$

$$y_2 = \frac{CLH}{LH+CLH} \qquad (3)$$

2.8. Graph neural network

As illustrated in Figure 1-C, the proposed architecture of the graph neural network consists of two graph convolution layers. The first convolution layer has an output channel dimension c of 5, while the second has an output channel dimension c of 1. A Tanh activation is applied after the convolution layers, and the resulting output is globally max-pooled to obtain a final positive score ratio. The neighborhood information is aggregated within the convolution operations. The ECConv graph convolution operator (Simonovsky & Komodakis, 2017) is considered, as in a prior work (Coupeau, Fasquel, Démas, Hertz-Pannier, & Dinomais, 2023), due to its ability to handle both node and edge attributes. Let $X^l(i)$ be the attribute of node i at layer $l \in [1,2]$ and $L(j,i)$ the attribute of the edge connecting structures i and j. The message passing at layer l can be defined as:

$$X^{l+1}(i) = \sigma\left(W^{l+1}X^l(i) + \sum_{j\in N(i)} F^{l+1}\left(L(j,i)\right)X^l(j)\right) \qquad (4)$$

where σ denotes the Tanh function, $W^{l+1} \in \mathrm{R}^{c\times 1}$ is a matrix of trainable weights and $\mathrm{F}^{l+1}: \mathrm{R} \rightarrow \mathrm{R}^{c\times 1}$ is a differentiable function (a multi-layer perceptron). $N(i)$ represents all nodes j that are neighboring i (i.e., connected to i). The global max pool operator then returns a graph-level output by taking the channel-wise maximum across the node dimension, so that its output (the predicted score ratio) is computed by: $y = \max_{i\in V} \mathrm{X}^2$ (i).

The network was implemented in a Python environment using the PyTorch Geometric library (Fey & Lenssen, 2019). The model was trained with Adam (Adaptive Moment Estimation) over 250 epochs with a learning rate $l_r = 0.001$. A mean-squared error (MSE) loss function was considered. Two GNNs were trained, one for predicting score y_1 and the other for predicting y_2 (both introduced previously). In both cases, a leave-one-out cross-validation strategy is implemented to test our method on all the children while managing the small size of the available dataset. Thus, in all cases, the model was trained on 34 graphs and tested on the remaining graph.

2.9. Evaluation

We evaluated the variation in structural characteristics (volumes, elongations, and distances) between the control group and the NAIS group to highlight the differences revealed by our method's graphs. This was a preliminary step to validate the relevance of the selected attributes.

Then, to assess the performance of the method, we measured the L1 distance or Manhattan distance, defined as the absolute difference between the predicted and actual score ratios. L1 distance emphasizes cases where the score prediction deviates significantly from the actual result. To analyze the prediction accuracy, we considered the mean, median, and maximum L1 distances.

We used Spearman's rank correlation coefficient (Caruso & Cliff, 1997) to measure the linear correlation between the predicted and actual score ratios since the sample did not follow a normal distribution according to a Shapiro-Wilk test. The Spearman correlation coefficient is defined as:

$$\rho = 1 - \frac{6\sum_{i=1}^{n} d_i^2}{n(n^2-1)} \qquad \text{with} \qquad d_i = (x_i - y_i) \qquad (5)$$

where n is the number of matched pairs of ranking, i.e. of measures (35 in our case), and d_i is the rank difference of the "i-th" element. Significance was determined at $p < 0.05$.

To evaluate the influence of each structural information (volume, elongation, and distances) on the prediction, we measured these metrics for various graph configurations (removing some or all of the structural relationships).

3. Results

Table 2 compares the structural characteristics (volumes, elongations, and distances) between control and NAIS participants. Note that the normalized volume has been multiplied by a factor of 1000 to avoid handling too small values (close to zero) during the graph convolution (eq.1).

Regarding volumes, we observe a decrease in the volume of structures in the lesioned hemisphere of NAIS participants, which confirms the results of previous studies (Hassett, Carlson, Babwani, & Kirton, 2022) (Ilves, et al., 2022). Additionally, there appears to be a slight increase in volumes in the contra-lesional hemisphere, as already reported in studies of the contra-lesional thalamus after perinatal stroke (Craig, Carlson, & Kirton, 2019).

Table 2. Comparison of the structural characteristics between the control group and the NAIS group (separated by left and right injury) by brain structure. The volumes listed are the brain structure volume multiplied by a factor of 1000 and normalized by TIV. The elongations indicated correspond to the brain structure elongation normalized by head circumference. Last part of the table displays the distances (in mm) between the centroids of supposedly symmetrical structures. The distance ratio L(i,j) corresponds to the edge attributes. Bold values indicate characteristics that exhibit significant variability compared to the control group, particularly in terms of standard deviation.

	Controls	**NAIS**		
		Left injured	**Right injured**	
Number	n=31	n=20	n=15	
Structural characteristics	**Mean (std)**	**Mean (std)**	**Mean (std)**	**p-value†**
Volumes ($x10^3$)				
Left thalamus	5.35 (±0.28)	**4.61 (±0.98)**	5.64 (±0.37)	< 0.001
Right thalamus	5.27 (±0.28)	**5.43 (±0.68)**	**4.96 (±0.55)**	0.025
Left caudate	3.13 (±0.26)	**2.65 (±0.99)**	3.37 (±0.34)	0.009
Right caudate	2.95 (±0.23)	3.01 (±0.29)	**2.88 (±0.61)**	0.497
Left putamen	3.70 (±0.21)	**3.00 (±1.21)**	4.02 (±0.35)	< 0.001
Right putamen	3.60 (±0.20)	**3.90 (±0.51)**	**3.42 (±0.71)**	0.019
Left pallidum	0.72 (±0.05)	**0.64 (±0.17)**	0.78 (±0.07)	0.008
Right pallidum	0.71 (±0.05)	0.76 (±0.07)	0.69 (±0.11)	0.014
Elongations				
Left thalamus	0.75 (±0.02)	**0.70 (±0.06)**	0.76 (±0.02)	< 0.001
Right thalamus	0.75 (±0.02)	0.75 (±0.03)	**0.72 (±0.04)**	0.112
Left caudate	0.91 (±0.04)	**0.85 (±0.15)**	0.93 (±0.04)	0.064
Right caudate	0.91 (±0.04)	0.91 (±0.03)	0.92 (±0.05)	0.959
Left putamen	0.81 (±0.03)	**0.74 (±0.14)**	0.82 (±0.03)	0.004
Right putamen	0.80 (±0.03)	0.80 (±0.03)	0.79 (±0.04)	0.745
Left pallidum	0.42 (±0.01)	**0.40 (±0.03)**	0.42 (±0.01)	0.018
Right pallidum	0.43 (±0.01)	0.43 (±0.01)	**0.41 (±0.02)**	0.091
Distances (mm) / Edge attribute L				
Thalamus	20.75 (±1.20) / 1.04 (±0.04)	**21.54 (±2.25) / 1.08 (±0.08)**	21.21 (±1.66) / **1.07 (±0.05)**	0.138
Caudates	23.25 (±1.53) / 1.05 (±0.04)	**24.92 (±2.59) / 1.09 (±0.09)**	**24.51 (±2.52) / 1.09 (±0.08)**	0.123
Putamen	44.52 (±1.83) / 1.03 (±0.02)	44.83 **(±3.37) /** 1.05 (±0.05)	**45.25 (±2.15) /** 1.04 (±0.02)	0.195
Pallidum	31.64 (±1.61) / 1.04 (±0.03)	**32.65 (±2.36) / 1.06 (±0.06)**	**32.62 (±1.89) /** 1.05 (±0.04)	0.148

†P-values are obtained by one-way Kruskal Wallis non-parametric ANOVA.

The lesioned hemisphere also shows a reduction in structures elongation compared to controls (with an average reduction between 0.02 and 0.07 for children with left injury). Elongations in the contra-lesioned hemisphere appear similar to the elongations of control participants (except

for the left caudate). Both structural characteristics (volume and elongation) were found to be correlated, according to Spearman's rho correlation coefficient ($\rho = 0.476, p = 1.25e^{-4}$ averaged over all brain structures). Logically, structural atrophy translates into structural contraction. However, elongation can provide additional information to our model by emphasizing variations between connected nodes.

The information regarding the distance between structures shows an increase in distances to centroids in NAIS participants compared to controls. This results in higher average ratios (particularly for the distance between the thalamus and the caudate) carried by the edges of the graph. In our GNN model, we expect that the higher distance ratio in NAIS participants will accentuate the difference between the characteristics of the node corresponding to the structure in the lesioned hemisphere (with lower volume and elongation) and its neighbor corresponding to its supposed symmetric in the contra-lesioned hemisphere (with higher volumes and elongations). Distances were not found to be correlated with volumes or elongations differences between hemispheres, according to Spearman's rho coefficient ($p > 0.05$). We can therefore assume that distances will provide additional information regarding basal ganglia/thalami deformation.

3.1. Basal ganglia structure and clinical motor function of the affected hand (y_1 prediction)

Figure 2 represents the predicted score ratio (y_1) of the affected hand using our model according to the actual score ratio. The GNN-based approach shows a positive correlation with the actual score ratio (ρ = 0.769, p = $6.62e^{-8}$). The model accurately predicts the score ratio of the affected hand compared to the 'unaffected' hand with a mean L1 distance of 0.027 (Table 3).

The score ratio of the affected hand, predicted from graphs that integrate only volume information, exhibits a significant positive correlation with the actual score ratio of the affected hand (ρ = 0.537, p = $8.81e^{-4}$). Additionally, the maximum L1 distance of the prediction is reduced to 0.095 according to Table 3. Combining volumes information with distances only or

elongations only reduces the correlation coefficient, but is still significant ($\rho = 0.476$, $p = 3.88e^{-3}$ for volumes and distances, $\rho = 0.373$, $p = 2.72e^{-2}$ for volumes and elongations). It

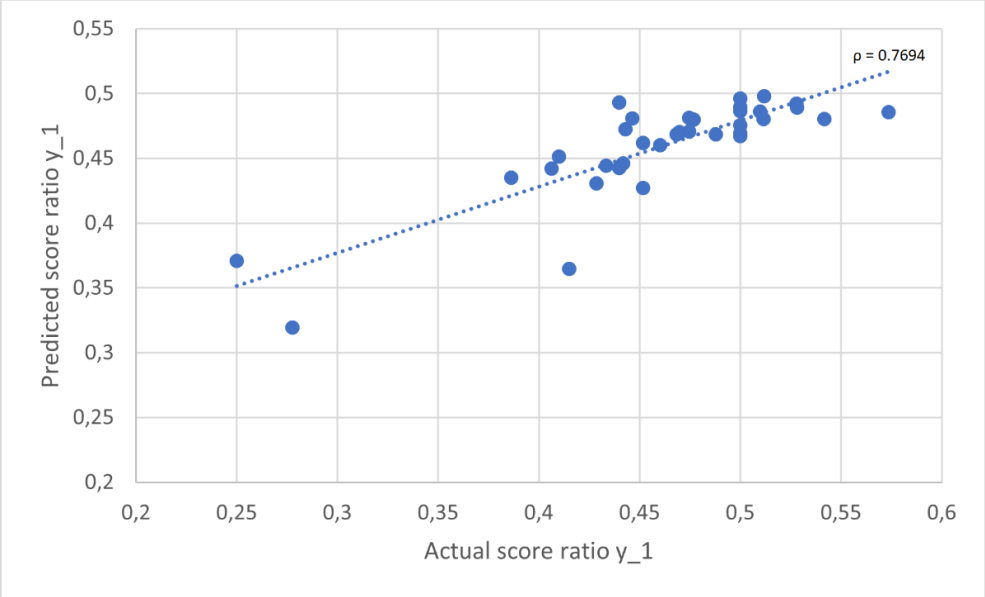

Figure 2. Predicted score ratio correlation with actual score ratio of the affected hand.

also decreases the accuracy of the prediction (mean L1 = 0.033 and 0.037, respectively).

The consideration of distances alone does not accurately predict the score ratio (mean L1= 0.047), which is close to the prediction obtained without considering any structural information (no attributes).

The best performances are achieved when all three structural information attributes are combined (all attributes).

Table 3. BBT Prediction for the affected hand

	Mean L1	**Median L1**	**Max L1**	**Spearman coefficient ρ (p-value)**
No attributes	0.046	0.037	0.221	-0.560 ($4.62e^{-4}$)
Distances	0.047	0.035	0.222	-0.654 ($2.04e^{-5}$)
Elongations	0.040	0.031	0.112	0.276 ($1.10e^{-1}$)
Volumes	0.031	0.027	**0.095**	0.537 ($8.81e^{-4}$)
Volumes + Distances	0.033	0.028	0.117	0.476 ($3.88e^{-3}$)
Elongations + Distances	0.036	0.030	0.108	0.288 ($9.34e^{-2}$)
Volumes + Elongations	0.037	0.033	0.103	0.373 ($2.72e^{-2}$)
All attributes	**0.027**	**0.024**	0.121	**0.769 ($6.62e^{-8}$)**

3.2. Basal ganglia structure and clinical motor function of the 'unaffected' hand (y_2 prediction)

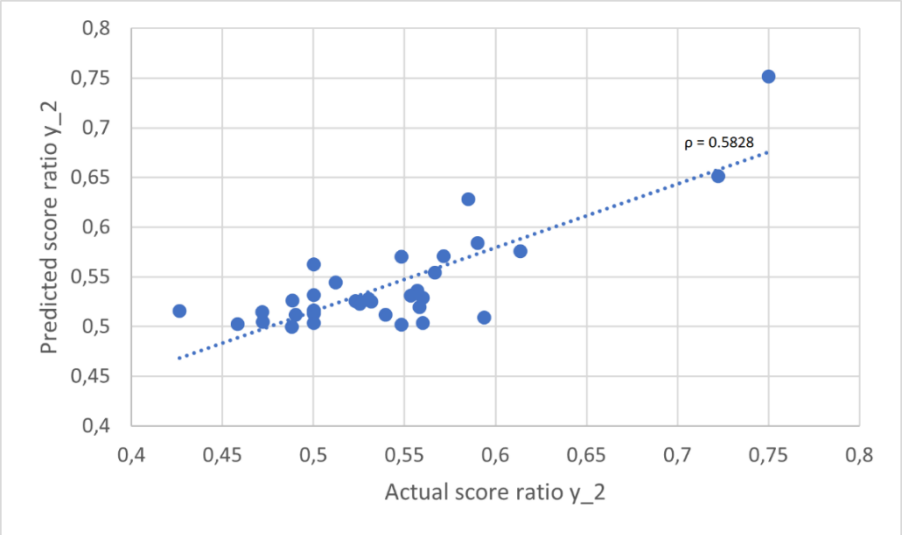

Figure 3. Predicted score ratio correlation with actual score ratio of the unaffected hand.

Figure 3 depicts the predicted score ratio of the 'unaffected' hand (y_2) compared to the actual score ratio. The GNN-based method's prediction of the score ratio of the 'unaffected' hand has a positive correlation with the actual score ratio ($\rho = 0.583$, $p = 2.39e^{-4}$). The model accurately predicts the score ratio of the 'unaffected' hand compared to the affected hand with a mean L1 distance of 0.028 (Table 4). This accuracy is consistent with that achieved for the affected hand.

Table 4. BBT Prediction for the unaffected hand

	Mean L1	**Median L1**	**Max L1**	**Spearman coefficient ρ (p-value)**
No attributes	0.046	0.035	0.223	-0.718 ($1.20e^{-6}$)
Distances	0.039	0.028	0.155	0.428 ($1.04e^{-2}$)
Elongations	0.030	0.025	**0.086**	0.563 ($4.23e^{-4}$)
Volumes	0.044	0.036	0.210	0.295 ($8.51e^{-2}$)
Volumes + Distances	0.041	0.039	0.191	0.529 ($1.09e^{-3}$)
Elongations + Distances	0.033	0.028	0.104	0.337 ($4.74e^{-2}$)
Volumes + Elongations	0.031	**0.022**	0.115	0.493 ($2.63e^{-3}$)
All attributes	**0.028**	0.023	0.089	**0.583 ($2.39e^{-4}$)**

The score ratio of the ‘unaffected’ hand, predicted from graphs that integrate only elongation information, also shows a positive correlation (Figure 4) with the actual score ratio of the ‘unaffected’ hand ($\rho = 0.563$, $p = 4.23e^{-4}$) and decreases the maximum L1 distance of the prediction to 0.086, as shown in Table 4.

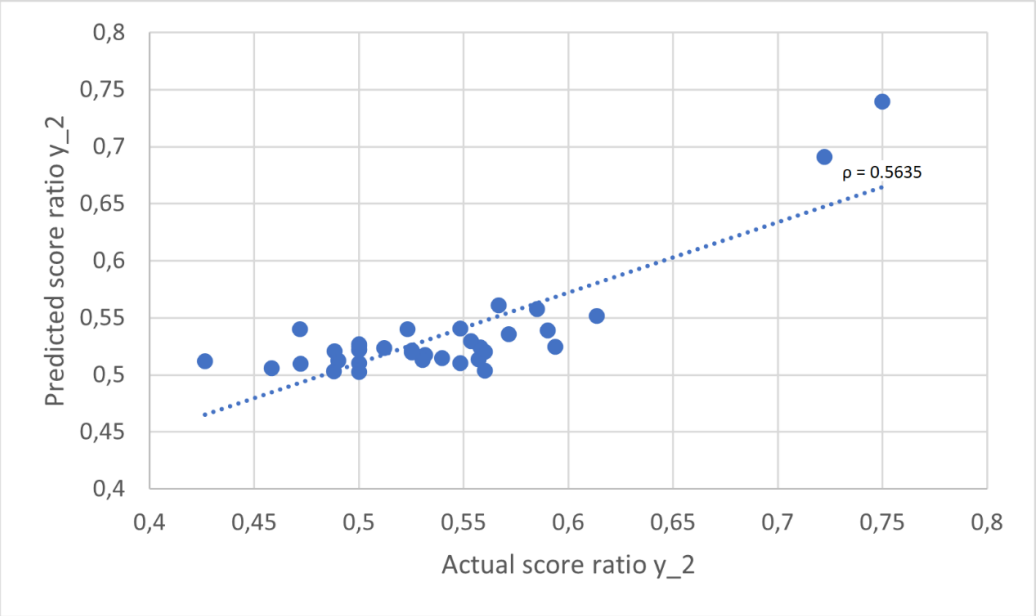

Figure 4. Predicted score ratio correlation with actual score ratio of the unaffected hand considering elongations only.

The correlation with the actual score ratio of the ‘unaffected’ hand considering the volumes or the distances alone is almost not significant ($p = 8.51e^{-2}$ and $p = 1.04e^{-2}$ respectively) and do not significantly enhance the L1 distance when compared to the model without any structural information (Table 4). Combining both information (volumes and distances) in the graph structure, does not significantly improve the L1 distance. However, combining this set of information with elongation improves the accuracy of the model’s prediction (in terms of L1 distance). Thus, the best median L1 distance is achieved by combining volume and elongation (median L1 = 0.022), and the best mean L1 distance is obtained when considering all three structural information (mean L1 = 0.028). Note that the high negative correlation between the score prediction without any attribute and the actual score ratio ($\rho = -0.718$, $p = 1.20e^{-6}$) reflects a very slight variation of the predicted scores. The model always predicts a score ratio of around 0.530, which is the average score ratio of the training data. The prediction is imprecise, as confirmed by the results of the L1 distance.

4. Discussion

In this work, our aim is to predict the motor function (evaluated through a BBT score) of both hands of children following early brain lesion. To achieve this, we utilize a graph neural network (GNN) to analyze the structural organization of the basal ganglia and thalamus (volumes, elongations, and distances), modeled as a graph, and solve a graph regression problem. The results indicate a significant correlation between the predicted score ratios and the actual score ratios for both hands ($\rho = 0.769$ for the affected hand and $\rho = 0.583$ for the 'unaffected' hand), together with a high accuracy in its predictions (mean L1 distance < 0.03). One important finding of this study is the importance of considering the whole macrostructural organization of the basal ganglia and thalami networks, rather than just their volume, to predict hand motor function. This study is the first, to our knowledge, to demonstrate a robust association between the structural characteristics of the basal ganglia and thalamus and the motor function of the 'unaffected' hand.

The results of the prediction raise questions about certain aspects when considering the diverse configurations of the graphs, with different amounts of structural information. We found a strong association between the volume information of the basal ganglia and thalamus and the affected hand motor function, as assessed by the BBT score ratio. This result confirms previous research (Dinomais, et al., 2016) (Ilves, et al., 2022) showing that volume loss of the basal ganglia and thalamus is associated with poor hand function after neonatal stroke. Our previous work has also demonstrated that the volume of the mediodorsal thalamus, among other structures, is associated with the BBT score of the contra-lesioned (or affected) hand. The decrease in volume of the basal ganglia and thalamus after NAIS may be due to neuronal loss (resulting from Wallerian degeneration following NAIS in MCA territory) or reduced dendritic arborization. Indeed, the volume of deep grey matter structures increases by approximately 105% by the end of the first year after birth (Gilmore, et al., 2012). Typical development of the thalamus and BG involves an increase in volume during early childhood, with peak growth occurring between late childhood and mid-adolescence (Narvacan, Treit, Camicioli, Martin, & Beaulieu, 2017). However, lesion at an early stage (here, at birth) can have a negative impact on the growth of these structures. Thus, the reduction in volume of ipsilesional structures is primarily due to decreased neuronal density resulting from the earlier explained neuronal loss. These distant (regarding the direct lesion) atrophies, known as diaschisis are well described after perinatal stroke (Kirton, et al., 2016) (Craig, Carlson, & Kirton, 2019).

In addition to volume, we have found a correlation between the motor function of the affected hand and the structural characteristics of the BG and thalamus including their shape (represented by their elongation) and the distances between supposedly symmetrical structures. This emphasizes the importance of the macrostructural characteristics of these deep brain structures in motor function. This shows that hand motor functions following neonatal stroke are influenced not only by the loss of volume in the basal ganglia and thalamus due to atrophy, but also by the deformation of these brain structures. Volume is not always a sensitive enough metric to accurately quantify a morphological change such as contraction.

Even if distances alone are not sufficient to predict both hand functions, combining them with other structural information (volume and elongation) improves the score ratio prediction. Moreover, graphs that include all attributes (including distances) perform better than those that only include volume and elongation information (Table 3 and Table 4). We can assume that considering distances as a ratio to the average distances D in control children is insufficient for distinguishing children. Since these distance ratios are small (often < 1.2), they have minimal impact on the graph regression. Yet, this information is still valuable when combined with the other structural information because it can help identify abnormal spatial organization (e.g., asymmetry) during the graph convolution of the GNN. Moreover, we have shown an increase in distances among the NAIS population compared to the control group, likely due to deformation at a distance from the infarct site, notably in the lesioned hemisphere. These results highlight the importance of preserving the global structure of the BG and thalami to maintain hand motor function after early brain lesion. This indirectly confirms the vulnerability of these deep grey matter structures to early brain lesion (Loh, et al., 2017) and their role in contributing to and modulating motor functions.

The results suggest that local morphometric changes in the BG and thalamus such as elongation and distances, in addition to volume changes, strongly influence hand motor function. For the 'unaffected' hand, these elongation characteristics are more closely linked to the motor function than the volume of these structures. This finding is supported by our results (Table 4) but it is difficult to explain. Variations in brain development following a unilateral lesion in both hemispheres (i.e., lesioned, and contra-lesioned hemispheres) may be related. Additionally, the contra-lesioned hemisphere, despite being considered 'healthy' by definition still suffers from the consequences of neonatal stroke. This confirms a previous conclusion stating that: "*Neonatal stroke does not appear to be only a focal lesion but a lesion that impacts the whole developing brain"* (Al Harrach, et al., 2021).

Regarding our results, we found a relationship between motor functions in both hands and the macrostructural organization of the basal ganglia and thalamus. Optimal function, specifically in motor control, is associated not only with the volume of these brain structures but also with their shape and inter-hemispherical distances. The three macrostructural information considered appear to be complementary. Sometimes, removing one set of data results in worse outcomes than using only one set of information. For example, in the 'unaffected' hand, the model based on elongation alone performs better than the one based on elongation and distances while in the affected hand, model based on volume alone performs better than combined with distances. This raises a possible « Goldilocks principle » for brain motor function relationships (Bigler, 2015).

This paper focuses on highlighting the potential use of assessing the macrostructural characteristics, including elongations and distances (thus not limited to volume), of the basal ganglia and thalamus in MRI as an early biomarker for predicting motor function in both hands after early brain lesion. However, this study has limitations that should be discussed along with future work to address them.

First, we assess the hand motor function of children after NAIS by using the Box and Blocks Test (BBT), which only evaluates gross manual dexterity. In future work, we plan to investigate the potential correlation between the macrostructural organization of the BG/thalamus and fine hand motor function, which can be evaluated using adapted tests such as the Nine Hole Peg Test (Smith, Hong, & Presson, 2000).

In this study, only children who underwent NAIS were assessed using the Box and Blocks Test. This is a limitation in our work, as we would like to verify whether the relationship observed between the macrostructural organization of the basal ganglia/thalami and motor skills is also present in control participants.

Another limitation of our study is the prediction of the BBT score normalized by the score of both hands. While this normalization may be sufficient to avoid fluctuations due to individual variabilities encountered in the raw BBT results, it is not yet optimal. Normalizing the score of each hand based on a complete neuropsychological evaluation could help to better overcome the impact of external factors (cognitive, behavioral, and motivational) on the motor performance.

Then, we could discuss the limited sample size. Nevertheless, our study cohort is comparable in size to other studies investigating NAIS (Hassett, Carlson, Babwani, & Kirton, 2022) (Lee,

et al., 2005) and was already considered for previous work (Al Harrach, et al., 2019) (Al Harrach, et al., 2021) (Dinomais, et al., 2016). Moreover, this is a unique homogeneous cohort in terms of patients' characteristics (term newborns aged 7 years), lesion characteristics (precise timing of the injury in the neonatal period, infarct localization in the MCA territory), and imaging conditions (monocentric data acquisition using a 3T MRI scanner). Therefore, our results are not blurred by the developmental consequences of prematurity, the diversity in the acquisition of motor skills with age, or experimental multicenter acquisition variability. When training the GNN, the leave-one-out cross-validation training strategy seems sufficient to mitigate the impact of limited training data. This may be explained by the GNN's relatively simple architecture (around only 100 trainable parameters), therefore less sensitive to the training dataset size, compared to architectures involving thousands of parameters.

Finally, we observed a correlation between volume and elongation features in the graph structure. However, GNN models struggle with covariation between features, especially in deep models (Chen, et al., 2020). To address this issue, we considered a simple architecture consisting of only 2 convolutional layers. However, we could use a framework as proposed recently (Jin, Liu, Ma, Aggarwal, & Tang, 2022) to handle better feature covariations, filter out redundant information in the graphs, and improve model robustness and predictions.

5. Conclusion

The hand motor function of children following neonatal stroke is correlated with the macrostructural organization (volume, elongation, distances) of the basal ganglia and thalami, rather than with the volume of these structures alone. The structural information differently influences the motor function of each hand, with the affected hand being more correlated with the volume and the 'unaffected' hand with the elongation of the structures. Highly accurate prediction of a BBT score ratio for both hands (mean L1 distance < 0.03) is achievable through a graph regression strategy. This strategy utilizes a graph neural network that operates on graphs modeling the inter-hemispheric macrostructural organization of the basal ganglia and thalami. These findings support the exploration of macrostructural features of the basal ganglia and thalami on MRI as an early biomarker for predicting motor function in both hands after early brain injury.

Acknowledgements

We sincerely thank the patients and their families for participating in this research. We also extend our gratitude to Rochelle Marsh for proofreading the English language.

Funding

This research was supported by the University Hospital of Angers (EudraCT number 2010-A00976-33), the *Ministry of Solidarity and Health* (EudraCT number 2010-A00329-30), and the *Fondation de l'Avenir* (ET0-571). The sponsors of the study did not play a role in the study design, data collection, data analysis, data interpretation, writing of the report, or decision to submit for publication.

Competing interests

The authors report no competing interests.

References

Al Harrach, M., Pretzel, P., Groeschel, S., Rousseau, F., Dhollander, T., Hertz-Pannier, L., . . . Dinomais, M. (2021). A connectome-based approach to assess motor outcome after neonatal arterial ischemic stroke. *Annals of Clinical and Translational Neurology, 8*(5), 1024-1037. doi:10.1002/acn3.51292

Al Harrach, M., Rousseau, F., Groeschel, S., Wang, X., Hertz-Pannier, L., Chabrier, S., . . . Dinomais, M. (2019). Alterations in cortical morphology after neonatal stroke: compensation in the contralesional hemisphere? *Developmental Neurobiology, 79*(4), 303-316. doi:10.1002/dneu.22679

Arsalidou, M., Duerden, E. G., & Taylor, M. J. (2013). The centre of the brain: topographical model of motor, cognitive, affective, and somatosensory functions of the basal ganglia. *Human Brain Mapping, 34*(11), 3031-54. doi:10.1002/hbm.22124

Bacciu, D., Errica, F., Micheli, A., & Podda, M. (2020). A gentle introduction to deep learning for graphs. *Neural Networks, 129*, 203-221. doi:10.1016/j.neunet.2020.06.006

Bigler, E. D. (2015). Structural Image Analysis of the Brain in Neuropsychology Using Magnetic Resonance Imaging (MRI) Techniques. *Neuropsychology Review, 25*(3), 224-249. doi:10. 1007/s11065-015-9290-0

Caruso, J. C., & Cliff, N. (1997). Empirical size, coverage, and power of confidence intervals for Spearman's rho. *Educational and psychological Measurement, 57*(4), 637-654. doi:10.1177/0013164497057004009

Chabrier, S., Pouyfaucon, M., Chatelin, A., Bleyenheuft, Y., Fluss, J., Gautheron, V., . . . Dinomais, M. (2019). From congenial paralysis to post-early brain injury developmental condition: Where does cerebral palsy

actually stand? *Annals of Physical and Rehabilitation Medicine, 63*(5), 431-438. doi:10.1016/j.rehab.2019.07.003

Chabrier, S., Saliba, E., Nguyen The Tich, S., Charollais, A., Varlet, M.-N., Tardy, B., . . . Landrieu, P. (2010). Obstetrical and neonatal characteristics vary with birthweight in a cohort of 100 term newborns with symptomatic arterial ischemic stroke. *European Journal of Paediatric Neurology, 14*, 206-213. doi:10.1016/j.ejpn.2009.05.004

Chen, D., Lin, Y., Li, W., Li, P., Zhou, J., & Sun, X. (2020). Measuring and relieving the over-smoothing problem for graph neural networks from the topological view. *Proceedings of the AAAI conference on artificial intelligence, 34*(4), 3438-3445. doi:10.1609/aaai.v34i04.5747

Coupeau, P., Fasquel, J.-B., Démas, J., Hertz-Pannier, L., & Dinomais, M. (2023). Detecting cerebral palsy in neonatal stroke children: GNN-based detection considering the structural organization of basal ganglia. *20th ISBI 2023-20th International Symposium on Biomedical Imaging.* Cartagena de Indias, Colombia: IEEE. doi:hal-04092356

Craig, B. T., Carlson, H. L., & Kirton, A. (2019). Thalamic diaschisis following perinatal stroke is associated with clinical disability. *Neuroimage Clinical, 21*, 101660. doi:10.1016/j.nicl.2019.101660

Dinomais, M., Hertz-Pannier, L., Groeschel, S., Chabrier, S., Delion, M., Husson, B., . . . Nguyen The Tich, S. (2015). Long term motor function after neonatal stroke: Lesion localization above all. *Human Brain Mapping, 36*, 4793-4807. doi:10.1002/hbm.22950

Dinomais, M., Hertz-Pannier, L., Groeschel, S., Delion, M., Husson, B., Kossorotoff, M., . . . Nguyen The Tich, S. (2016). Does Contralesional Hand Function After Neonatal Stroke Only Depend on Lesion Characteristics? *Stroke, 47*, 1647-1650. doi:10.1161/STROKEAHA.116.013545

Fey, M., & Lenssen, J. (2019). Fast Graph Representation Learning with PyTorch Geometric. *ICLR 2019 Workshop on Representation Learning on Graphs and Manifolds.* doi:10.48550/arXiv.1903.02428

Fluss, J., Dinomais, M., & Chabrier, S. (2019). Perinatal stroke syndromes: Similarities and diversities in aetiology, outcome and management. *European Journal of paediatric neurology, 23*(3), 368-383. doi:10.1016/j.ejpn.2019.02.013

Gilmore, J. H., Shi, F., Woolson, S. L., Knickmeyer, R. C., Short, S. J., Lin, W., . . . Shen, D. (2012). Longitudinal development of cortical and subcortical gray matter from birth to 2 years. *Cerebral Cortex, 22*(11), 2478-2485. doi:10.1093/cercor/bhr327

Hammers, A., Allom, R., Koepp, M. J., Free, S. L., Myers, R., Lemieux, L., . . . Duncan, J. S. (2003). Three-dimensional maximum probability atlas of the human brain, with particular reference to the temporal lobe. *Human Brain Mapping, 19*, 224-247. doi:10.1002/hbm.10123

Hanik, M., Demirtaş, M. A., Gharsallaoui, M. A., & Rekik, I. (2022). Predicting cognitive scores with graph neural networks through sample selection learning. *Brain Imaging and Behavior, 16*, 1123-1138. doi:10.1007/s11682-021-00585-7

Hassett, J., Carlson, H., Babwani, A., & Kirton, A. (2022). Bihemispheric developmental alterations in basal ganglia volumes following unilateral perinatal stroke. *Neuroimage Clinical, 35*, 103143. doi:10.1016/j.nicl.2022.103143

Hollander, E., Anagnostou, E., Chaplin, W., Esposito, K., Haznedar, M. M., Licalzi, E., . . . Buchsbaum, M. (2005). Striatal volume on magnetic resonance imaging and repetitive behaviors in autism. *Biological Psychiatry, 58*(3), 226-232. doi:10.1016/j.biopsych.2005.03.040

Husson, B., Hertz-Pannier, L., Renaud, C., Allard, D., Presles, E., Landrieu, P., & Chabrier, S. (2010). Motor outcomes after neonatal arterial ischemic stroke related to early MRI data in a prospective study. *Pediatrics, 126*, 912-8. doi:10.1542/peds.2009-3611

Ilves, N., Lõo, S., Laugesaar, R., Loorits, D., Kool, P., Talvik, T., & Ilves, P. (2022). Ipsilesional volume loss of basal ganglia and thalamus is associated with poor hand function after ischemic perinatal stroke. *BMC Neurology, 22*(1), 23. doi:10.1186/s12883-022-02550-3

Jin, W., Liu, X., Ma, Y., Aggarwal, C., & Tang, J. (2022). Feature overcorrelation in deep graph neural networks: A new perspective. *KDD '22: Proceedings of the 28th ACM SIGKDD Conference on Knowledge Discovery and Data Mining*, 709-719. doi:10.1145/3534678.3539445

Jongbloed-Pereboom, M., Nijhuis-van der Sanden, M. G., & Steenbergen, B. (2013). Norm scores of the box and block test for children ages 3-10 years. *American Journal of Occupational Therapy, 67*, 312-8. doi:10.5014/ajot.2013.006643

Kirton, A. (2013). Modeling developmental plasticity after perinatal stroke: defining central therapeutic targets in cerebral palsy. *Pediatric Neurology, 28*, 81-94. doi:10.1016/j.pediatrneurol.2012.08.001

Kirton, A., Williams, E., Dowling, M., Mah, S., Hodge, J., Carlson, H., . . . Ichord, R. (2016). Diffusion imaging of cerebral diaschisis in childhood arterial ischemic stroke. *International Journal of Stroke, 11*(9), 1028-1035. doi:10.1177/1747493016666089

Kuczynski, A. M., Kirton, A., Semrau, J. A., & Dukelow, S. P. (2018). Bilateral reaching deficits after unilateral perinatal ischemic stroke: a population-based case-control study. *Journal of NeuroEngineering and Rehabilitation, 15*(1), 77. doi:10.1186/s12984-018-0420-9

Lee, J., Croen, L. A., Lindan, C., Nash, K. B., Yoshida, C. K., Ferriero, D. M., . . . Wu, Y. M. (2005). Predictors of outcome in perinatal arterial stroke: a population-based study. *Annals of Neurology, 58*(2), 303-308. doi:10.1002/ana.20557

Loh, W. Y., Anderson, P. J., Cheong, J. L., Spittle, A. J., Chen, J., Lee, K. J., . . . Thompson, D. K. (2017). Neonatal basal ganglia and thalamic volumes: very preterm birth and 7-year neurodevelopmental outcomes. *Pediatric Research, 82*(6), 970-978. doi:10.1038/pr.2017.161

Makropoulos, A., Aljabar, P., Wright, R., Hüning, B., Merchant, N., Arichi, T., . . . Rueckert, D. (2016). Regional growth and atlasing of the developing human brain. *NeuroImage, 125*, 456-478. doi:10.1016/j.neuroimage.2015.10.047

Narvacan, K., Treit, S., Camicioli, R., Martin, W., & Beaulieu, C. (2017). Evolution of deep gray matter volume across the human lifespan. *Human Brain Mapping, 38*(8), 3771-3790. doi:10.1002/hbm.23604

Oldfield, R. C. (1971). The assessment and analysis of handedness: the edinburgh inventory. *Neuropsychologia, 9*, 97-113. doi:10.1016/0028-3932(71)90067-4

Peterson, B. S., Vohr, B., Staib, L. H., Cannistraci, C. J., Dolberg, A., Schneider, K. C., . . . Ment, L. R. (2000). Regional brain volume abnormalities and long-term cognitive outcome in preterm infants. *The Journal of the American Medical Association, 284*(15), 1939-1947. doi:10.1001/jama.284.15.1939

Pietschnig, J., Penke, L., Wicherts, J. M., Zeiler, M., & Voracek, M. (2015). Meta-analysis of associations between human brain volume and intelligence differences: How strong are they and what do they mean? *Neuroscience and Biobehavioral Reviews, 57*, 411-432. doi:10.1016/j.neubiorev.2015.09.017

Raju, T. N., Nelson, K. B., Ferriero, D., & Lynch, J. K. (2007). Ischemic perinatal stroke: summary of a workshop sponsored by the National Institute of Child Health and Human Development and the National Institute of Neurological Disorders and Stroke. *Pediatrics, 120*, 609-619. doi:10.1542/peds.2007-0336

Raznahan, A., Shaw, P. W., Lerch, J. P., Clasen, L. S., Greenstein, D., Berman, R., . . . Giedd, J. N. (2014). Longitudinal four-dimensional mapping of subcortical anatomy in human development. *Proceedings of the National Academy of Sciences of the United States of America, 111*(4), 1592-1597. doi:10.1073/pnas.1316911111

Sandman, C. A., Head, K., Muftuler, L. T., Su, L., Buss, C., & Davis, E. P. (2014). Shape of the basal ganglia in preadolescent children is associated with cognitive performance. *NeuroImage, 99*, 93-102. doi:10.1016/j.neuroimage.2014.05.020

Simonovsky, M., & Komodakis, N. (2017). Dynamic edge-conditioned filters in convolutional neural networks on graphs. *Conference on Computer Vision and Pattern Recognition (CVPR)* (pp. 3693-3702). IEEE/CVF. doi:10.1109/CVPR.2017.11

Smith, Y. A., Hong, E., & Presson, C. (2000). Normative and validation studies of the nine-hole peg test with children. *Perceptual and Motor Skills, 90*, 823-843. doi:10.2466/pms.2000.90.3.823

Yushkevich, P. A., Gao, Y., & Gerig, G. (2016). ITK-SNAP: An interactive tool for semi-automatic segmentation of multi-modality biomedical images. *2016 38th Annual International Conference of the IEEE Engineering in Medicine and Biology Society (EMBC)*, (pp. 3342-3345). doi:10.1109/EMBC.2016.7591443